J. Fluid Mech. (2017), *vol.* 824, *pp.* 688–700.
doi:10.1017/jfm.2017.360

Liquid-infused surfaces as a passive method of turbulent drag reduction

M. K. Fu[1,†], I. Arenas[2], S. Leonardi[3] and M. Hultmark[1]

[1]Department of Mechanical and Aerospace Engineering, Princeton University, 41 Olden St, Princeton, NJ 08544, USA

[2]Department of Mathematical Sciences, The University of Texas at Dallas, 800 W Campbell Rd, Richardson, TX 75080, USA

[3]Department of Mechanical Engineering, The University of Texas at Dallas, 800 W Campbell Rd, Richardson, TX 75080, USA

(Received 17 February 2017; revised 18 April 2017; accepted 19 May 2017; first published online 10 July 2017)

Liquid-infused surfaces present a novel, passive method of turbulent drag reduction. Inspired by the Nepenthes Pitcher Plant, liquid-infused surfaces utilize a lubricating fluid trapped within structured roughness to facilitate a slip at the effective surface. The conceptual idea is similar to that of superhydrophobic surfaces, which rely on a lubricating air layer, whereas liquid-infused surfaces use a preferentially wetting liquid lubricant to create localized fluid–fluid interfaces. Maintaining the presence of these slipping interfaces has been shown to be an effective method of passively reducing skin friction drag in turbulent flows. Given that liquid-infused surfaces have only recently been considered for drag reduction applications, there is no available framework to relate surface and lubricant characteristics to any resulting drag reduction. Here we use results from direct numerical simulations of turbulent channel flow over idealized, liquid-infused grooves to demonstrate that the drag reduction achieved using liquid-infused surfaces can be described using the framework established for superhydrophobic surfaces. These insights can be used to explain drag reduction results observed in experimental studies of lubricant-infused surfaces. We also demonstrate how a liquid-infused surface can reduce drag even when the viscosity of the lubricant exceeds that of the external fluid flow, which at first glance can seem counter-intuitive.

Key words: drag reduction, turbulence simulation, turbulent flows

1. Introduction

Liquid-infused surfaces (LIS) are proposed as a novel, passive method of turbulent drag reduction. Analogous to superhydrophobic surfaces (SHS), LIS are composed of a lubricant that is trapped within chemically matched roughness elements and is immiscible with external fluids. Where SHS rely on the Lotus leaf effect by deriving their properties from the presence of air pockets within the surface topography, LIS are inspired by the Nepenthes Pitcher Plants, which rely on the movement of

† Email address for correspondence: mkfu@princeton.edu

liquid lubricants to facilitate mobility of the fluid–fluid interfaces. In each case, a heterogeneous surface is formed, comprising both solid–fluid and fluid–fluid interfaces. The choice of a liquid lubricant enables LIS to exhibit numerous beneficial properties for naval applications including anti-biofouling (Epstein *et al.* 2012) and ice-phobicity (Kim *et al.* 2012). In contrast to superhydrophobic surfaces, which are typically susceptible to hydrostatic pressure, liquid-infused surfaces also exhibit extreme pressure stability (Wong *et al.* 2011). The presence of this trapped fluid is also instrumental in facilitating passive drag reduction. Under shear, the mobility of the fluid within the roughness allows the fluid–fluid interface to maintain a finite velocity. The collection of the localized slipping interfaces yields a non-zero, streamwise slip velocity at the effective interface. A wide range of SHS studies (Fukagata, Kasagi & Koumoutsakos 2006; Daniello, Waterhouse & Rothstein 2009; Park, Park & Kim 2013; Rastegari & Akhavan 2015) have established this effect as the primary mechanism by which SHS are expected to reduce drag in turbulent flows.

Although numerous experiments have quantified the drag reduction capabilities of SHS, (Truesdell *et al.* 2006; Daniello *et al.* 2009; Park, Sun & Kim 2014), it has only recently been demonstrated that LIS are able to reduce drag in laminar (Solomon, Khalil & Varanasi 2014) and turbulent (Rosenberg *et al.* 2016) flows. Although the lubricating fluids are quite different, the drag reducing mechanisms are fundamentally the same for both SHS and LIS. A common modelling approach for SHS is to simply consider a pattern of shear-free and no-slip regions, and to neglect the effects of fluid properties and surface features within the air layer. While this model neglects the details of the flow within the cavity, the leading-order physics and effects on the external flow can still be replicated. For SHS, such a simplification might be justifiable as the dynamic viscosity of water is $\sim$55 times larger than that of air, but it is inappropriate for LIS, as the lubricant will typically have a viscosity of the same order as the external fluid. Consequently, predicting the drag reduction from a LIS requires a more detailed understanding of the interaction between the lubricant, structural roughness and external flow.

Here, laminar flow results for liquid-infused surfaces are synthesized and extended into the turbulent regime to parameterize the design and performance of idealized, grooved liquid-infused surfaces. Using direct numerical simulations (DNS) of turbulent channel flow over idealized, liquid-infused grooves, a regime can be found where the effective slip length and drag reduction are accurately modelled from surface and flow parameters. Despite the increased detail and complexity of the heterogeneous boundary, the drag reduction derived from such surfaces is found to be consistent with slip drag reduction results and models from the superhydrophobic literature. Furthermore, the surfaces are well characterized with an effective slip length found to agree with laminar flow models in a regime consistent with that established by Seo & Mani (2016). From the framework and experiments presented here, it can be shown that drag reduction can be achieved even when the viscosity of the lubricating fluid exceeds the external fluid viscosity.

1.1. *Drag reduction framework*

In contrast to SHS, it is necessary to understand the coupling between the lubricant flow within the roughness and the external fluid to determine the effects of the finite lubricant viscosity in LIS, see figure 1. Recirculation of the fluid lubricant supports a finite interfacial velocity. Locally along the interface, the external and lubricating fluids must both exhibit the same slip velocity, U_s, and shear stress. Alternatively, we

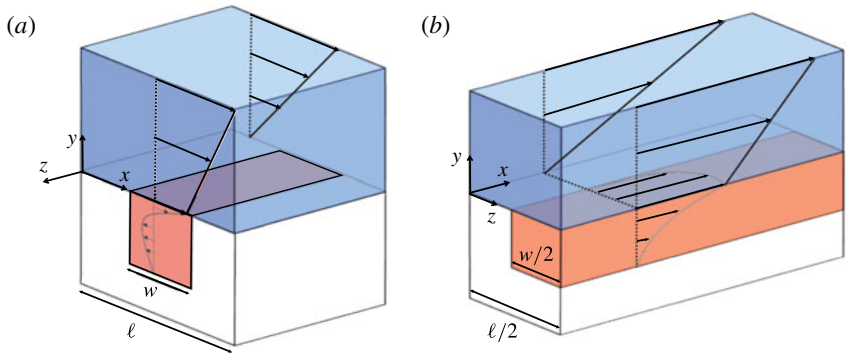

FIGURE 1. (Colour online) Illustration of fluid flow within LIS cavities in a spanwise groove configuration (*a*) and streamwise groove configuration (*b*). Two configurations of grooved LIS surfaces are considered. Blue represents the external fluid with dynamic viscosity μ_{ext}, while red represents the lubricant with a lower dynamic viscosity μ_{int}.

can express the second matching condition at the interface, denoted as location i, in the following manner

$$N \left.\frac{\partial U_{ext}}{\partial y}\right|_i = \left.\frac{\partial U_{int}}{\partial y}\right|_i, \tag{1.1}$$

with the viscosity ratio, N, defined as the ratio of the viscosity of the external fluid, μ_{ext}, to that of the infused liquid, μ_{int}, given by $N = \mu_{ext}/\mu_{int}$. Also, $\partial U/\partial y$ is defined as the surface-normal gradient of the streamwise velocity for the respective fluids. Due to the presence of the slip velocity, the external flow will have a smaller local velocity gradient over the fluid–fluid interface compared to the flow over the no-slip regions. From equation (1.1) it is clear that if the lubricating and external fluids exhibit different dynamic viscosities, there will be a discontinuity in the velocity gradient at the interface. As the viscosity within the cavity is decreased, and N is increased, the fluid–fluid interface is able to sustain a higher slip velocity; specifically, in the limit when $N \to \infty$, we expect the fluid–fluid interface to behave as a shear-free boundary.

Understanding effective drag reduction over LIS involves aggregating all of the individual, localized slipping effects along the fluid–fluid interfaces as a macroscopic boundary condition for the flow. Given the inherent complexity in considering the full, heterogeneous boundary, it is typically assumed that one can homogenize the surface and simply consider the surface averaged or effective slip velocity (Lauga & Stone 2003), $\langle U_s \rangle$, over the surface. In the case of surfaces exhibiting periodic patterning (e.g. stripes or grooves), surface-wise averaging can be considered over a pattern period. Equivalently, it is usually more convenient to consider the effective slip length, $b \equiv \langle U_s \rangle \langle \partial U_{ext}/\partial y|_i \rangle^{-1}$, where $\langle \partial U_{ext}/\partial y|_i \rangle$ denotes the surface-normal gradient of the mean streamwise velocity evaluated at the effective interface. In the current work, where the flow is turbulent, $\langle\,\rangle$ denotes averaging both in time and space. The effective slip length, b, can be rigorously defined as the distance into a surface where the no-slip condition would be satisfied by a linear extrapolation of average velocity gradient at the interface.

Generally, the magnitude of drag reduction derived from a slip surface is governed by the ratio of b to the nominal length scale of the shear. As the ratio between these

two length scales increases, so does the drag reduction. For laminar flows, where the shear is usually determined from the domain geometry, drag reduction can be related explicitly to b and known parameters. Unfortunately, a relationship is not as straightforward for turbulent flows. It is currently understood that the drag reduction is not solely governed by b, but by the non-dimensional slip length, b^+, given as $b^+ \equiv bu_\tau \nu^{-1}$, where the friction velocity, u_τ, is defined in the conventional manner with respect to the wall shear stress, $\tau_w = \rho u_\tau^2$, where ρ and ν denote the fluid density and kinematic viscosity, respectively (Park *et al.* 2013; Rastegari & Akhavan 2015; Srinivasan *et al.* 2015). This relationship has been demonstrated using direct numerical simulations of turbulent channel flow by Park *et al.* (2013), where the drag reduction over shear-free stripes of various widths and area fractions was found to collapse with b^+. This relationship has also been validated experimentally by Srinivasan *et al.* (2015) using a turbulent Taylor–Couette apparatus with superhydrophobic cylinders. Several models have been derived to predict the drag reduction associated with a given b^+, typically by applying the slip as an offset to the mean velocity profile (Fukagata *et al.* 2006; Busse & Sandham 2012; Rastegari & Akhavan 2015). The model presented by Rastegari & Akhavan (2015) considers on the drag reduction associated with streamwise slip, while Fukagata *et al.* (2006) and Busse & Sandham (2012) utilize results from numerical simulations to model drag increasing features such as spanwise slip. Each model indicates that a larger b^+ will generate increased drag reduction. Importantly, such a relationship is encouraging for high Reynolds number applications where, assuming that the lubricating layer can be retained, the drag reduction from a given surface will increase with the flow shear stress. To evaluate if LIS reduce drag in a manner consistent with a slip surface, we have performed DNS of turbulent channel flow over idealized liquid infused surfaces. The width and depth of the square grooves is 5 % of the channel half-height. Both streamwise and transverse configurations of the grooves are considered. For both the streamwise and spanwise configurations, two different levels of lubricant filling were considered. The first configuration of LIS considered the lubricant filled exactly to the crest plane, while the second configuration considers the grooves are filled and covered by a thin film of lubricant. In each case the fluid–fluid interface does not deform (i.e. the interfacial tension between the fluid and lubricant is assumed to be infinitely large). Here we consider simulations conducted at $Re_\tau = u_\tau h \nu^{-1} \approx 180$, where h is the channel half-height.

2. Numerical details and flow configuration

In these simulations, the flow over canonical grooved surfaces, consisting of square bars infused with a second, fully wetting and immiscible, liquid with viscosity ratio from $N = 10^{-1}$ to $N = 10^2$ was studied, where $N = 0.1$, 1, 2.5, 10, 20 and 100. The width (w) and depth of the roughness elements are equal and constant for all the simulations ($w = 0.05h$ where h is the half-height of the channel). For both transversal square bars and longitudinal square bars the width to pitch (ℓ) ratio is $w/\ell = 0.5$. The Reynolds number, $Re = \rho_{ext} U_b h/\mu_{ext} = 2800$, corresponds to $Re_\tau = 180$ when both walls are smooth, where U_b is the bulk streamwise velocity. The flow rate has been kept constant in all simulations. To quantify the effect of the position of the interface on the drag, three cases have been computed: the interface placed at the crests plane and $0.05w$ above and below the crests plane, although the analysis presented above relies only on the first two configurations. The displacement of the interface corresponds to about 0.5 wall units for a $Re_\tau = 180$ for a smooth channel.

The computational box, illustrated in figure 2, is $6.4h \times 2.05h \times 1.6h$ and the computational grid is $1024 \times 512 \times 256$, each in the streamwise, surface-normal and spanwise direction. The additional $0.05h$ increase in channel height corresponds to the cavity height of the textured surfaces. A non-uniform grid is used in the surface-normal direction with 40 points clustered within the roughness. Periodic boundary conditions apply in the streamwise and spanwise directions for both the upper and lubricating fluids while the no-slip condition is imposed on both walls. At the interface, continuity of the shear stress $\mathrm{d}U/\mathrm{d}y$ and zero surface-normal velocity is imposed to mimic a stable interface and flow in Cassie state corresponding to a high surface tension. In high Reynolds numbers flows, interfacial deformations will become important, however, the choice of a flat interface is to understand the consequences of using a finite viscosity lubricant compared to the typical treatments of superhydrophobic surfaces as no-slip/shear-free patterns (which also assume flat interfaces). Furthermore, this approximation will be considered reasonable for surfaces when the interfacial tension dominates the interfacial dynamics. For example, the interfacial Weber number in Rosenberg *et al.* (2016) was found to be $We = \rho u_\tau^2 w \gamma^{-1} = O(10^{-3})$, where γ is the interfacial tension between the lubricant and external fluid. Statistics are computed with about 300 velocity fields, 2 non-dimensional time units apart (time is normalized by h/U_b). After the first 3000 non-dimensional time units, which were discarded when processing the data, convergence to a statistically steady state was achieved.

Results were obtained by solving the incompressible, dimensionless Navier–Stokes and continuity equations which can expressed concisely, using index notation, as:

$$\frac{\partial u_i}{\partial t} + \frac{\partial u_i u_j}{\partial x_j} = -\frac{\partial p}{\partial x_i} + \frac{1}{Re}\frac{\partial}{\partial x_j}\left[\widetilde{\mu}(\phi)\left(\frac{\partial u_i}{\partial x_j} + \frac{\partial u_j}{\partial x_i}\right)\right] + \Pi\delta_{i1} + f\delta(\phi), \tag{2.1}$$

$$\frac{\partial u_i}{\partial x_i} = 0, \tag{2.2}$$

respectively. Here, $i = 1$ denotes the streamwise direction, $i = 2$ is the surface-normal direction and $i = 3$ is the spanwise direction, Π is the pressure gradient required to maintain a constant flow rate, ϕ is the signed distance from the interface and f is the force at the interface between the two fluids in normal direction to the interface. The distance function, ϕ, is used to distinguish between the two fluids and it appears also in the factor $\widetilde{\mu}$, defined as $\widetilde{\mu}(\phi) = 1 + (N^{-1} - 1)H(\phi)$, where H is the Heaviside function, which is $H = 0$ when $\phi < 0$ (external fluid) and $H = 1$ when $\phi > 0$ (internal fluid).

The force at the interface, f, is computed to prescribe a $u_2 = 0$ condition with $f\delta(\phi) = 0$ at any other point not lying on the interface. The Navier–Stokes equations have been discretized in an orthogonal coordinate system using the staggered central second-order finite-difference approximation. Details of the numerical method can be found in Orlandi (2000). The discretized system is advanced in time using a fractional-step method with viscous terms treated implicitly and convective terms explicitly. At each time step, the momentum equations are advanced with the pressure at the previous step, yielding an intermediate non-solenoidal velocity field. A scalar quantity, Φ, projects the non-solenoidal field onto a solenoidal one. A hybrid low-storage third-order Runge–Kutta scheme is used to advance the equations in time. The structure of the grooves is treated by the immersed boundary technique described in detail by Orlandi & Leonardi (2006).

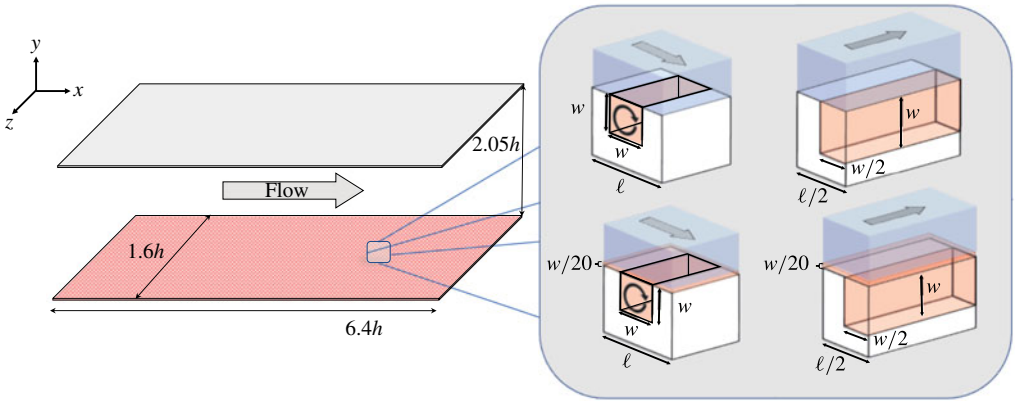

FIGURE 2. (Colour online) Diagram of the computational domain and LIS surface configuration. Illustration of the four configurations for liquid-infused surfaces. From upper left moving clockwise: spanwise filled to crest, streamwise filled to crest, streamwise overfilled and spanwise overfilled. Dimensions are $w = 0.5\ell = 0.05h$. Overlying film thickness is $0.05w$.

3. Results

If the idealized LIS surfaces reduce drag through a streamwise slip at the interface, as hypothesized, the drag reduction measured in the DNS should demonstrate the same correlation to b^+ as slip surfaces such as those in Min & Kim (2004) and Busse & Sandham (2012) as well as patterned shear-free surfaces like those in Park *et al.* (2013) and Rastegari & Akhavan (2015). Figure 3 shows the correlation between b^+ and the measured drag reduction for the idealized LIS for values of N ranging from $N = 10^{-1}$ to $N = 10^2$ which are compared to the correlation from Park *et al.* (2013) and the theoretical prediction from Rastegari & Akhavan (2015). Encouragingly, the results from the current study demonstrate the same correlation between b^+ and the drag reduction that has been established in the literature for SHS. Conspicuously, there are notable cases for small values of b^+ where there is a drag increase. Most of these instances correspond to transverse grooves filled to crest plane. These results are consistent with the observations of Woolford *et al.* (2009), where superhydrophobic surfaces composed of transverse grooves were found to generate a drag increase.

Homogenization of the heterogeneous LIS boundary into a single, effective parameter b is convenient for several reasons. While we wish to discern how effective different surfaces are for reducing drag, the performance of any given surface will vary for different flow conditions and facilities. To good approximation, b behaves as a flow independent parameter, provided it is not significantly larger than the viscous length scale, νu_τ^{-1} (Park *et al.* 2013; Srinivasan *et al.* 2015; Seo & Mani 2016). By using DNS of channel flow over idealized SHS, Seo & Mani (2016) found that when $b^+ < 5$, b could effectively be characterized with the b derived in the Stokes flow limit. Consequently, in this limit, the flow dependence of the drag reduction can be separated from the dependence on surface properties. This allows us to reduce our problem to characterizing how b varies with N, and ultimately, describes the effect on drag reduction more generally.

Here, we hypothesize that the conclusions of Seo & Mani (2016) extend to LIS as well. We can then utilize Stokes flow relations to model b for turbulent flows when

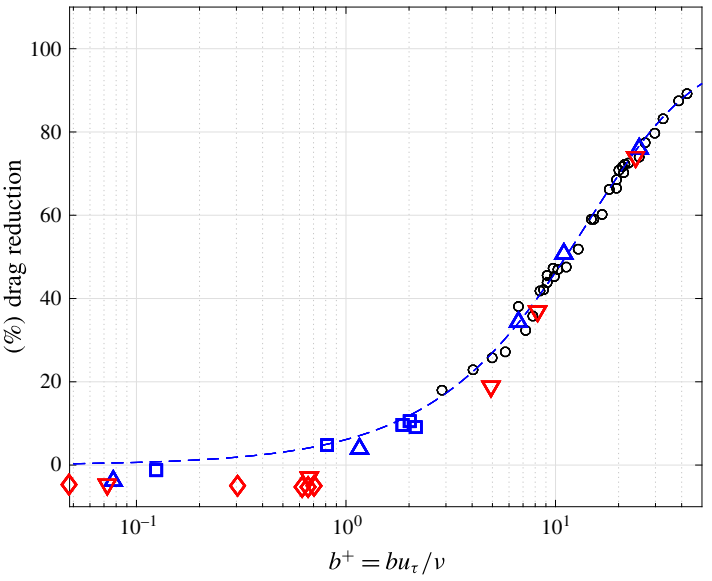

FIGURE 3. (Colour online) Drag reduction results of turbulent channel DNS at $Re_\tau \approx 180$ as a function of b^+. Drag reduction is defined using the no-slip wall shear stress, τ_0, compared to that of a slip wall, τ_{LIS}, where % drag reduction $= 100 \times (1 - \tau_{LIS})\tau_0^{-1}$. Blue and red denote streamwise and spanwise configurations, respectively; (□, ◇): results from idealized LIS from present study with the lubricant filled to the crest plane; (△, ▽): results of idealized LIS where an overlying lubricant film ($0.05w$) is present; (○): results from Park *et al.* (2013) of turbulent channel flow DNS shear-free stripes; (––): prediction from Rastegari & Akhavan (2015) for drag reduction over shear-free stripes.

$b^+ < 5$. While there are numerous studies that have sought to model b for SHS in Stokes flow using canonical patterns of shear-free and no-slip regions (Philip 1972; Lauga & Stone 2003; Ybert *et al.* 2007), such models are insufficient for use with LIS, because the details of the flow within the cavity are largely neglected. Recent studies (Ng & Wang 2011; Schönecker *et al.* 2014) have characterized the effect of finite lubricant viscosity on b for wetted grooves (i.e. lubricant is filled to the crest plane of the grooves with no overlying film) in streamwise and transverse configurations such as those seen in figure 2. Of particular interest is the work of Schönecker *et al.* (2014) which derives explicit relationships for b in terms of N and surface geometry for grooved configurations. The effective slip length in Stokes flow, for wetted grooves, is given by:

$$b = \frac{\ell \ln\left(\sec\left(\frac{\pi a}{2}\right)\right)}{\left(c\pi + \frac{1}{2aDN}\ln\left(\frac{1+\sin\left(\frac{\pi a}{2}\right)}{1-\sin\left(\frac{\pi a}{2}\right)}\right)\right)}, \tag{3.1}$$

where ℓ denotes the periodicity of the grooves in the transverse direction, a gives the exposed liquid area fraction and D is the normalized local maximum slip length at the centre of the grooves. The constant c is $c = 1$ for streamwise and $c = 2$ for spanwise configurations. While this study considers grooves with square cross-sections, this model is applicable to any rectangular geometries with arbitrary aspect ratio

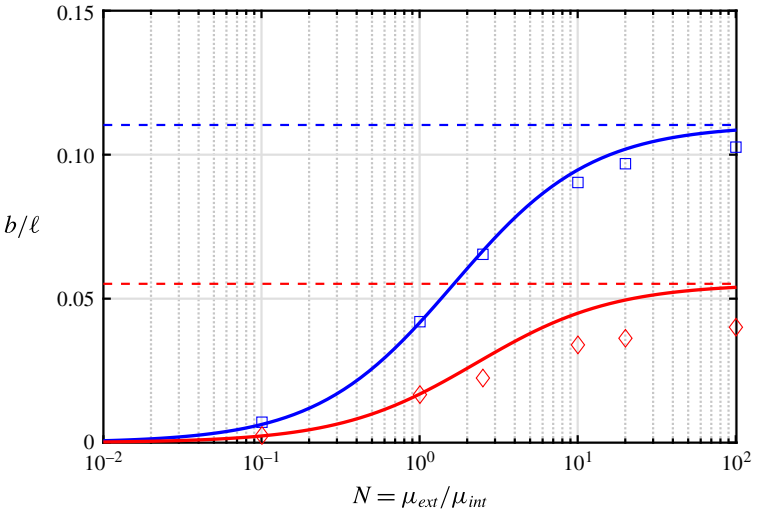

FIGURE 4. (Colour online) b/ℓ as a function of viscosity ratio, N, from DNS of turbulent channel flow at $Re_\tau \approx 180$ where one wall is replaced with streamwise (□) and spanwise (◇) grooves that are perfectly wetted with second liquid up to the crest plane. Results are compared to predictions from Stokes flow models of LIS from Schönecker, Baier & Hardt (2014) for both streamwise (–, blue) and spanwise (–, red) groove configurations as well as predictions from Philip (1972) for streamwise (– –, blue) and spanwise (– –, red) configurations of shear-free stripes. In both configurations, the exposed liquid area fraction is modelled assuming 50 % liquid area fraction.

(assuming a stable interface). The parameter D, which is determined from purely geometric properties of the surface, describes the depth of the uppermost eddy within the cavity and captures the influence of cavity aspect ratio on b. For aspect ratios larger than 0.5 (depth/width), both D and b are approximately constant to within a few per cent, however there is a rapid decrease in both D and b as below this aspect ratio.

If the results from Seo & Mani (2016) are applicable to LIS, we should find that replicating the LIS boundary condition from Schönecker *et al.* (2014) in a turbulent flow will yield the same b when $b^+ < 5$. From the turbulent DNS data set, we can select the results for which $b^+ < 5$ and evaluate their agreement with the prediction from the Stokes flow model. A comparison between the b from the turbulent DNS with the theoretical prediction from Stokes flow can be seen in figure 4. For the streamwise configuration, there is good agreement between the measured b in the turbulent flow and the Stokes flow prediction for that surface configuration. The agreement for values $N \leqslant 1$ is excellent and begins to overpredict slightly for values $N \gg 1$. This deviation most likely stems from the larger values of N equating to larger Re in the cavity, where the flow in the cavity begins to deviate slightly from the Stokes flow distributions. However, for the spanwise configuration, the overall agreement appears to be acceptable only when $N \leqslant 1$, while the model more significantly overestimates b as N increases. The finite Re flow in the spanwise cavities deviates more significantly from the Stokes flow approximation than their streamwise counterparts. This deviation is further compounded by the presence of significant spanwise slip. The spanwise orientation of the grooves means that the spanwise slip length of the surface is larger than the streamwise slip length. The

presence of the spanwise slip has been shown to strengthen the turbulent structures which serves to increase the drag over the surface (Min & Kim 2004; Fukagata *et al.* 2006). Consequently, the average wall shear is increased resulting in a smaller streamwise b. This effect becomes more pronounced with larger values of N, as an increase in N corresponds to a larger increase in the spanwise slip compared to the streamwise slip.

4. Discussion

An important limit to consider is $N \to \infty$ as the surface behaviour should mimic the behaviour of shear-free and no-slip stripes, such as those used in Park *et al.* (2013). In this limit, the details of the flow within the grooves are no longer important as the fluid–fluid interface begins to resemble a shear-free surface to the outer flow. Consequently, b of the surface is well approximated by that described by Philip (1972) and Lauga & Stone (2003) in the regime established by Seo & Mani (2016), as is indicated by the dashed lines in figure 4.

Particularly interesting is the ability to reduce drag using infused fluids with higher viscosity compared to the bulk flow. Consider the case of $N = 1$, where non-zero drag reduction was found in the numerical simulations. At first glance it might seem counter intuitive that a surface infused with a liquid of the same viscosity can reduce the drag. This effect is due to the interface that is imposed at the crest plane, altering the method of dissipation from turbulent dissipation, in the bulk flow, to Stokes flow dissipation within the cavity. Any infused lubricant with a finite viscosity will reduce the drag if the drag reduction introduced by the streamwise slip exceeds the additional viscous drag introduced by the lubricant flow within the roughness. Often times, even for $N \approx O(1)$, this exchange can yield a net drag reduction, although the magnitude of the drag reduction decreases rapidly when $N < 1$ as can be seen in figure 4. In the limit of $N \to 0$ the liquid-infused surface approaches the conventional no-slip surface.

In addition to variations in the viscosity ratio, N, the influence of an overlying film was also evaluated. A series of simulations where the grooves were overfilled with lubricant such that an film of lubricant was present over the crest of the groove walls. The thickness of the film, t, was 5 % of the cavity depth ($t = w/20$) in each case. One would expect that the presence of a film would provide additional drag reduction and correspondingly a larger b, since it completely isolates the external flow from the solid surface. This enhanced slip length due to an overlying film is analogous to the findings of Gao & Feng (2009), where the presence of a continuous gas layer over superhydrophobic grooves due to depinning of the contact line was shown to produce a significant increase in slip length. Without the presence of the grooves structure underneath, the slip length of this thin film along would be well approximated by the thickness of the film scaled with the N, where $b_{film} = ((N-1)w/20)$. One might expect that the effect of this film would be similar, even with the presence of underlying grooves. If this was the case, the b of the overfilled surface could be constructed by summing the individual b values associated with the film and the groove structured (e.g. the value given by (3.1)).

To evaluate the appropriateness of this low-order approximation, the b values from the DNS for overfilled, streamwise grooves were compared with the corresponding prediction using the additive model. The results are found in table 1. Noticeably, the values from the DNS are consistently underpredicted by the simple addition of each b for the film and grooves, with the discrepancy becoming more pronounced with increasing N. The placement of the interface above the crest plane means that the flow

N	b_{DNS}/ℓ	$b_{est}/\ell = b_{Stokes}/\ell + (N-1)(0.05w/\ell)$
0.1	−0.0106	$-0.0162 = (0.0063) + (-0.0225)$
1	0.0443	$0.0416 = (0.0416) + (0)$
10	0.3964	$0.3197 = (0.0947) + (0.2250)$
20	0.7546	$0.5769 = (0.1019) + (0.4750)$

TABLE 1. Comparison between the effective slip length from the DNS, b_{DNS}, of overfilled, streamwise grooves and the estimated slip length b_{est} using Stokes flow models and thin film approximation.

field in the groove is no longer accurately modelled by equation (3.1). A more refined model is needed to better describe the role of the overlying film in modifying the flow within the groove structure. However, despite the deficiencies in this approach, this conservative approximation reveals that not only does an overlying layer of lubricant provide a significant increase to the slip length, but that added contribution exceeds the expected slip length associated with a thin film alone.

4.1. *Comparison to experiments*

Given that utilizing LIS for drag reduction purposes is a relatively nascent concept, there are comparatively few experimental studies to quantify their drag reduction potential. The most relevant study to the authors' knowledge was conducted by Rosenberg *et al.* (2016) where threaded cylinders were infused with several liquid lubricants of different viscosities ($N = 0.03$, 0.67 and 2.7) and evaluated in a turbulent flow generated by a Taylor–Couette flow apparatus. Air ($N \approx 55$) was also tested as a lubricant to create a SHS with the same surface geometry as the LIS. Using the framework outlined above, we can compare the experimental results from the Taylor–Couette apparatus and compare them to the predictions from the framework presented above. Applying the methodology outlined by Srinivasan *et al.* (2015), we can estimate b for each of the LIS and SHS configurations. Comparing the slip surfaces to the no-slip case, the slip lengths can be approximated by assuming that b^+ can be applied as a on offset to the skin-friction law given by:

$$\sqrt{\frac{2}{C_f}} = M \ln(Re_\tau) + N + b^+, \tag{4.1}$$

where C_f denotes the skin-friction coefficient defined as $C_f = 2\tau\rho^{1-}U^{-2}$ with M and N being empirical, geometry-dependent constants analogous to the 'universal' von Kármán constant κ and the additive constant B for turbulent flat-plate (zero pressure gradient) boundary layers. Similar to the channel flow experiments, we define Re_τ as $Re_\tau = \Delta r U \nu^{-1}$, where Δr is gap distance between the inner and outer cylinders.

The comparison between the calculated b from Rosenberg *et al.* (2016) and the Stokes flow estimation can be seen in table 2. Conspicuously, the Stokes flow prediction tend to underpredict the estimates for b from the Taylor–Couette study, especially for the heptane lubricant. However, this discrepancy can best explained by the noted presence of the a lubricant film in the experimental study. The thickness of the lubricant film was estimated by weighing the dry cylinder and then the liquid-infused cylinder before and after the experiment to estimate the amount of lubricant retained in the grooves. The authors were then able to conclude that a

Lubricant	N	b_{exp} (μm)	b_{Stokes} (μm)
(1) FC3283	0.67	38	9
(2) Heptane	2.7	133	25
(3) Air (SHS)	55	68	55

TABLE 2. Values for b_{exp} were estimated from the results of Rosenberg *et al.* (2016) using the methodology of Srinivasan *et al.* (2015). The values were compared to values for b_{Stokes} from Schönecker *et al.* (2014) given by equation (3.1) using the rough approximation outlined in § 4 for calculating the slip length of streamwise grooved surfaces with an overlying layer of lubricant.

lubricant film of $O(1)$ μm was most likely present on the liquid-infused cylinders. The slip length models assume that the crest of the roughness features are completely exposed to the external flow, acting as no-slip surface. In contrast to the fluid–fluid interfaces, these no-slip portions are responsible for the bulk of the skin-friction drag. From the presented simulations, the presence of an overlying film is shown to have an effect on b exceeding that of the nominal thickness of the film. While one would expect that b of an overfilled, grooved surface would equate to the sum of the slip lengths from the Stokes flow prediction and an overlying film (nominally the film thickness weighted by N), the simulations indicate that this is not that case. The configuration of overfilled, streamwise grooves is a more effective drag reducing surface than the sum of the individual components (i.e. the film and filled grooves). The noted presence of a lubricant film on the cylinder can explain some of the difference in the magnitude of the slip lengths. The experimentally determined values exceed the prediction from Stokes flow for the grooved surface alone and highlights the importance of maintaining thin film on a LIS for drag reduction applications.

5. Conclusions

Using evidence from direct numerical simulations and turbulent Taylor–Couette flow experiments, a framework was presented that enables the design of drag reducing liquid-infused surfaces for turbulent flows. The drag reduction results from the DNS of turbulent channel flow over idealized LIS agree well with the slip drag reduction models derived for superhydrophobic surfaces and results of Park *et al.* (2013). Furthermore, a regime, corresponding to $b^+ < 5$, was found for lubricant filled streamwise grooves where b is well predicted by Stokes flow. Using the drag reduction models, this regime roughly corresponds to surfaces that would reduce drag up to approximately 20 %. This regime is consistent with the findings of Seo & Mani (2016) where a similar regime was found for patterned shear-free and no-slip surfaces. An important practical consideration is revealed by this analysis when comparing the potential of SHS and LIS. While it is clear that a larger value of N associated with the air in SHS is advantageous for increasing the drag reduction, there are diminishing returns once $N \gg 1$. For example, heptane is approximately 20 times more viscous than air, however, b of a LIS surface using a heptane lubricant is estimated to be half that of the equivalent SHS. While this viscosity penalty associated with choosing a liquid lubricant over air (i.e. SHS) would appear significant, the choice of a liquid can provide greater robustness against hydrostatic pressure and turbulent pressure fluctuations, a common failure mechanism for SHS. Furthermore, using larger feature size and spacing can increase b, compensating for the higher viscosity of the lubricant.

Importantly, while this effective streamwise slip velocity is the primary mechanism by which drag reduction is achieved, it will also serve to drain the lubricant from grooves, which effectively will set the upper limit for the drag reduction. Because the effective slip length and drag reduction is well predicted by the Stokes flow value, the relationship between the external shear stress and effective slip velocity can be determined *a priori*, and will serve as a surface design guideline.

Acknowledgements

The authors are thankful to all of the former and current members of the ONR MURI SLIPS team, especially to T. V. Buren, Professor H. Stone and Professor A. Smits for their insight and discussions. This work was supported under Office of Naval Research (ONR) Multidisciplinary University Research Initiative (MURI) grants N00014-12-0875 and N00014-12-1-0962, Program Manager Dr K.-H. Kim. This work was also supported, in part, by the Department of Defense (DoD) through the National Defense Science & Engineering Graduate Fellowship (NDSEG) Program. The numerical simulations were performed on the Texas Advanced Computing Center (TACC) and through the DOD High Performance Computing Modernization Program.

REFERENCES

BUSSE, A. & SANDHAM, N. D. 2012 Influence of an anisotropic slip-length boundary condition on turbulent channel flow. *Phys. Fluids* **24** (5), 055111.

DANIELLO, R. J., WATERHOUSE, N. E. & ROTHSTEIN, J. P. 2009 Drag reduction in turbulent flows over superhydrophobic surfaces. *Phys. Fluids* **21** (8), 085103.

EPSTEIN, A. K., WONG, T.-S., BELISLE, R. A., BOGGS, E. M. & AIZENBERG, J. 2012 From the cover: liquid-infused structured surfaces with exceptional anti-biofouling performance. *Proc. Natl Acad. Sci. USA* **109** (33), 13182–13187.

FUKAGATA, K., KASAGI, N. & KOUMOUTSAKOS, P. 2006 A theoretical prediction of friction drag reduction in turbulent flow by superhydrophobic surfaces. *Phys. Fluids* **18** (5), 051703.

GAO, P. & FENG, J. J. 2009 Enhanced slip on a patterned substrate due to depinning of contact line. *Phys. Fluids* **21** (10), 102102.

KIM, P., WONG, T. S., ALVARENGA, J., KREDER, M. J., ADORNO-MARTINEZ, W. E. & AIZENBERG, J. 2012 Liquid-infused nanostructured surfaces with extreme anti-ice and anti-frost performance. *ACS Nano* **6** (8), 6569–6577.

LAUGA, E. & STONE, H. A. 2003 Effective slip in pressure-driven Stokes flow. *J. Fluid Mech.* **489**, 55–77.

MIN, T. & KIM, J. 2004 Effects of hydrophobic surface on skin-friction drag. *Phys. Fluids* **16** (7), 0–3.

NG, C.-O. & WANG, C. Y. 2011 Effective slip for Stokes flow over a surface patterned with two- or three-dimensional protrusions. *Fluid Dyn. Res.* **43** (6), 065504.

ORLANDI, P. 2000 *Fluid Flow Phenomena*, 1st edn, vol. 55. Springer.

ORLANDI, P. & LEONARDI, S. 2006 DNS of turbulent channel flows with two- and three-dimensional roughness. *J. Turbul.* **7** (July 2015), N73.

PARK, H., PARK, H. & KIM, J. 2013 A numerical study of the effects of superhydrophobic surface on skin-friction drag in turbulent channel flow. *Phys. Fluids* **25** (11), 110815.

PARK, H., SUN, G. & KIM, C.-J. 2014 Superhydrophobic turbulent drag reduction as a function of surface grating parameters. *J. Fluid Mech.* **747**, 722–734.

PHILIP, J. R. 1972 Integral properties of flows satisfying mixed no-slip and no-shear conditions. *Z. Angew. Math. Phys.* **23**, 960–968.

RASTEGARI, A. & AKHAVAN, R. 2015 On the mechanism of turbulent drag reduction with super-hydrophobic surfaces. *J. Fluid Mech.* **773**, R4.

ROSENBERG, B. J., VAN BUREN, T., FU, M. K. & SMITS, A. J. 2016 Turbulent drag reduction over air- and liquid- impregnated surfaces. *Phys. Fluids* **28** (1), 015103.

SCHÖNECKER, C., BAIER, T. & HARDT, S. 2014 Influence of the enclosed fluid on the flow over a microstructured surface in the Cassie state. *J. Fluid Mech.* **740**, 168–195.

SEO, J. & MANI, A. 2016 On the scaling of the slip velocity in turbulent flows over superhydrophobic surfaces. *Phys. Fluids* **28** (2), 025110.

SOLOMON, B. R., KHALIL, K. S. & VARANASI, K. K. 2014 Drag reduction using lubricant-impregnated surfaces in viscous laminar flow. *Langmuir* **30** (36), 10970–10976.

SRINIVASAN, S., KLEINGARTNER, J. A., GILBERT, J. B., COHEN, R. E., MILNE, A. J. B. & MCKINLEY, G. H. 2015 Sustainable drag reduction in turbulent Taylor–Couette flows by depositing sprayable superhydrophobic surfaces. *Phys. Rev. Lett.* **114** (January), 014501.

TRUESDELL, R., MAMMOLI, A., VOROBIEFF, P., VAN SWOL, F. & BRINKER, C. J. 2006 Drag reduction on a patterned superhydrophobic surface. *Phys. Rev. Lett.* **97**, 044504.

WONG, T.-S., KANG, S. H., TANG, S. K. Y., SMYTHE, E. J., HATTON, B. D., GRINTHAL, A. & AIZENBERG, J. 2011 Bioinspired self-repairing slippery surfaces with pressure-stable omniphobicity. *Nature* **477**, 443–447.

WOOLFORD, B., PRINCE, J., MAYNES, D. & WEBB, B. W. 2009 Particle image velocimetry characterization of turbulent channel flow with rib patterned superhydrophobic walls. *Phys. Fluids* **21** (8), 085106.

YBERT, C., BARENTIN, C., COTTIN-BIZONNE, C., JOSEPH, P. & BOCQUET, L. 2007 Achieving large slip with superhydrophobic surfaces: scaling laws for generic geometries. *Phys. Fluids* **19**, 123601.